Journal of NUCLEAR SCIENCE and TECHNOLOGY, Vol. 47, No. 10, p. 849–852 (2010)

RAPID COMMUNICATION

Distribution of Microbubble Sizes and Behavior of Large Bubbles in Mercury Flow in a Mockup Target Model of J-PARC

Katsuhiro HAGA[1,*], Takashi NAOE[1], Hiroyuki KOGAWA[1], Hidetaka KINOSHITA[1], Masato IDA[1], Masatoshi FUTAKAWA[1], Bernard W. RIEMER[2], Mark W. WENDEL[2], David K. FELDE[2] and Ashraf A. ABDOU[2]

[1]*Japan Atomic Energy Agency, Toukai-mura, Naka-gun, Ibaraki 319-1195, Japan*
[2]*Oak Ridge National Laboratory, Oak Ridge TN, USA*

(Received March 11, 2010 and accepted in revised form April 30, 2010)

KEYWORDS: mercury spallation target, microbubble injection, J-PARC, cavitation damage, pressure wave, bubble size distribution, beam window, mercury loop test, TTF

I. Introduction

The high-power pulsed spallation neutron source of the Japan Proton Accelerator Research Complex (J-PARC) started its operation in May 2008, and it is now used as one of the most powerful facilities in the world for research in the most advanced fields of material and life sciences.[1)] However, there are some hindrances to achieving full-power operation at 1 MW. The most significant is the cavitation problem. When the short-pulse high-power proton beam is injected into the mercury target, pressure waves are generated by the abrupt thermal expansion of mercury, which may cause cavitation damage to the target vessel wall. Because cavitation damage degrades the structural integrity and seriously decreases the lifetime of the target vessel,[2,3)] technologies to mitigate pressure waves have been crucially needed.

Microbubble injection into mercury is one of the prospective technologies to mitigate the pressure wave, and the effect of microbubbles has been investigated experimentally and numerically.[4–7)] The injected microbubbles are expected to absorb the thermal expansion of the mercury at the heat source location, and attenuate the pressure wave during the propagation process.[4,5)] Okita *et al.* showed by numerical simulations that bubbles with radius less than 100 μm are desirable to mitigate pressure waves effectively.[4)] To realize these effects, several difficulties must be overcome. First of all, microbubbles must be properly distributed in the area of the peak heat load, which is the source location of strong pressure waves. Since liquid mercury has a higher density than liquid water, microbubbles should be subject to strong buoyancy, and hence, controlling the bubble distribution in flowing mercury may be difficult. The other concern is that the essential cooling of the target vessel by the mercury might be degraded by the injected gas. Since the thermal diffusivity of gases is much lower than that of liquid mercury, accumulated gas layers attached to the surface of the vessel walls could significantly decrease the cooling performance.

In this paper, we report the preliminary results of a mercury loop test using a mockup model of the target vessel, performed as one of the studies for a mercury target design with a bubbling system. This experiment was carried out under collaboration with the Oak Ridge National Laboratory (ORNL) using their Target Test Facility (TTF), which is an actual-scale mercury loop constructed for the mercury target development at ORNL. We performed mercury flow experiments to investigate the bubble flow phenomena in the actual target size of J-PARC. We report here the measured bubble size distribution and several interesting phenomena observed in the experiments. One of the difficulties in using liquid mercury comes from its opacity: one cannot see gas bubbles in mercury by optical techniques. In the present experiment, injected microbubbles in contact with the transparent top wall were observed to determine the bubble size distribution in the target vessel. A large void area formed at a downstream flow vane is also reported.

II. Experiment

1. Experimental Setup

Figure 1 shows the schematic view of the mockup model of the mercury target. The dimensions of the model are 961 mm in length, 545 mm in width, and 220 mm in height. Because the mercury flow field and the bubble rising motion due to buoyancy were considered to be the dominant factors that determine the bubble distribution, the arrangement of the flow vanes and the size of the model were made almost the same as those of the actual target. The forefront wall of the target vessel, where a proton beam is injected, is called the beam window. Because the beam window is very close to the source location of strong pressure waves, it is the place most vulnerable to cavitation damage. Thus, distributing microbubbles around the beam window is the most important point to mitigate pressure waves effectively. The top

*Corresponding author, E-mail: haga.katsuhiro@jaea.go.jp

©Atomic Energy Society of Japan

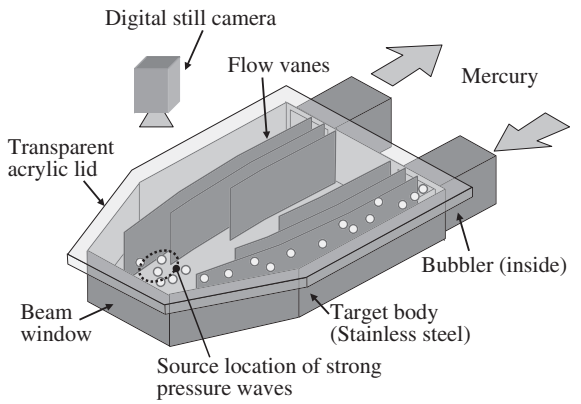

Fig. 1 Schematic view of the mockup model

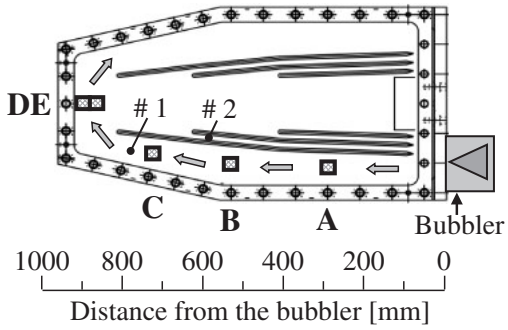

Fig. 2 Measuring position on the mockup model

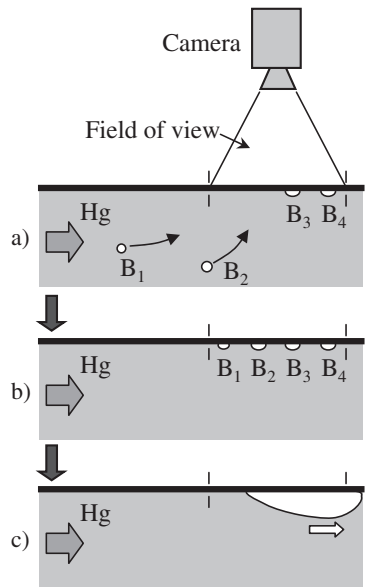

Fig. 3 Schematic motion of bubbles appearing on the top wall

wall of the mockup model was made of transparent acrylic plates to observe the bubbles rising to the inner surface of the top wall. The transparent acrylic top wall is 50 mm thick to endure an internal pressure of 1 MPa required by the TTF safety rules. The side walls were made with a flat plate to simplify the model structure, while the actual target has rounded side walls. The bubble generator, hereafter called bubbler, was installed at the mercury inlet. A swirl-type bubbler was used in this experiment. The performance of the swirl-type bubbler was evaluated in a small mercury loop in advance, where microbubbles from several tens to several hundreds micrometers in radius were generated. Pressure gages were mounted at the inlet and outlet of the bubbler and the outlet of the target vessel.

2. Experimental Conditions and Techniques

The experiment was carried out at mercury flow rates of 5 and 7.5 L/s, while the mercury flow rate of the actual system is 11.4 L/s. These flow rates correspond to mercury velocities of 0.5, 0.75, and 1.14 m/s at the target model inlet, respectively. 5 L/s was determined sufficient to maintain microbubble generation. 7.5 L/s was the limit determined based on the pressure loss at the bubbler to maintain its structural integrity because it was made of synthetic resin. The amount of helium supplied to the bubbler was 0.1% (in volume percent) of the mercury flow, which was an optimum value for bubbler performance. The microbubbles were generated and scattered by the swirl-type bubbler continuously; hence, the bubble distribution at the outlet of the bubbler was assumed to be quasi-homogeneous.

Images of the bubbles on the inner surface of the top wall were taken with a digital still camera, which was a Nikon D200 with a Micro Nikkor lens (105 mm) and a teleconverter mounted on it. The shutter interval was 0.2 s and the shutter speed was 1/8,000 s. An extra light source was used to obtain proper brightness. Images were taken at the five positions A to E along the main stream channel numbered as #1 in **Fig. 2**; #2 indicates the inner flow channel.

Figure 3 shows the bubble motion schematically. The dimension of the field of view was $33 \times 22\,\mathrm{mm}^2$. B_1 and B_2 in Fig. 3(a) are the free bubbles flowing in mercury and appear in the field of view when they reach the top wall in Fig. 3(b). We wanted to count the number of such free bubbles in the image. On the other hand, B_3 and B_4 are bubbles clinging to the top wall all the way, whose origins are not clear. After new free bubbles reached the top wall one after another and the number increased in the field of view, a large gas slug passed through the field and most of the small bubbles were cleared, as shown in Fig. 3(c). This was the repeating pattern of bubble behavior in the image. Thus, only the bubbles that newly appeared in the image were counted as the valid data to abstract free bubbles like B_1 and B_2. Because of the obtuse contact angle of mercury on the wall, the size of the bubble clinging to the wall surface appears larger than that of the free bubble. This effect was taken into consideration to convert the bubble sizes on the image to the free bubble sizes. Because the bubbles with radii up to several hundred micrometers were of interest, bubbles larger than 1 mm were not counted. Bubbles appearing in the field of view in 1 s, which included five sequential images, were counted to obtain the bubble size distribution at each position of the target model.

III. Results and Discussion

1. Bubble Size Distribution in the Introductory Channel

Figure 4 shows the bubble radius distribution measured at positions A, B, and C in Fig. 2. Because these positions are

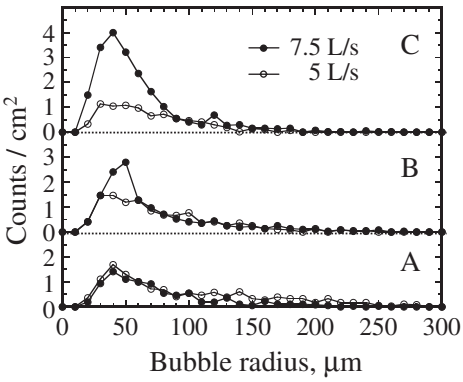

Fig. 4 Bubble size distribution at positions A, B, and C (Helium supply: 0.1% of mercury flow rate)

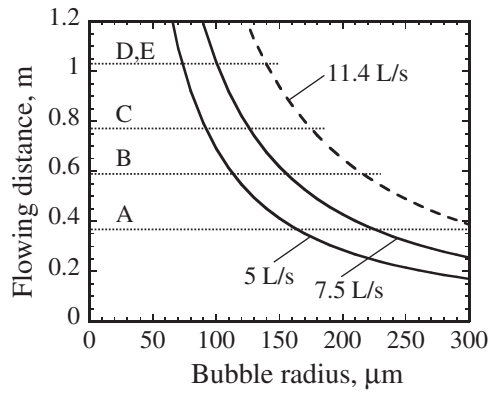

Fig. 5 Flowing distance of bubbles from the bubbler

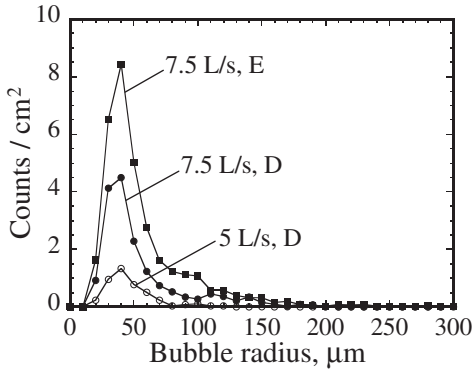

Fig. 6 Bubble size distribution at positions D and E (Helium supply: 0.1% of mercury flow rate)

located along a straight single channel of the main stream of mercury, the fundamental behavior of bubbles can be observed without disturbances. It can be seen that the bubbles with the radius larger than 150 μm are very few in all cases, while the small bubbles around the radius of 40 μm were formed. In the case of 7.5 L/s, it can be seen that the number of bubbles increased in the range from 10 to 90 μm, and the peak shape became sharp as the position went downstream from A to C, which indicates that the bubbles in those size ranges are most likely to be transported further. In the case of 5 L/s, a notable peak rise was not observed.

In order to understand the reason underlying these results, we evaluated the reachable distance of bubbles L, using the following equation:

$$L = \frac{h}{u} V. \tag{1}$$

Here, h is the height of the mercury flow channel of the target model, which is 80 mm, u is the terminal rising velocity of a bubble, and V is the mercury flow velocity. Bubbles were assumed to rise from the bottom to the top of the target model in order to evaluate the maximum reachable distance. Because no data was available for the terminal rising velocity of microbubbles in mercury, we used the empirical equation of Peebles and Garber.[8)]

$$u = 0.33 g^{0.76} \left(\frac{\rho}{\mu}\right)^{0.52} R^{1.28} \tag{2}$$

g is gravitational acceleration, ρ is liquid density, μ is liquid viscosity, and R is bubble radius. Peebles and Garber measured the terminal rising velocity of bubbles in 22 liquids, although mercury was not included, and formulated it taking the liquid properties such as density, viscosity, and surface tension into consideration. **Figure 5** shows the calculated flowing distance versus the bubble radius. Assuming that the bubbles that rise to the top wall do not go back into the mercury bulk flow again, it can be understood that bubbles with the radius larger than 230 μm do not reach the downstream region of position A as free bubbles. The size of the reachable bubble decreases as the position goes downstream, and finally, at position C, only the bubbles with the radius smaller than 130 μm can exist. Although the actual bubble flow is strongly affected by the mercury turbulence and coalescences, this simple calculation could estimate qualitatively the range of reachable bubble sizes shown in Fig. 4 fairly well.

2. Bubble Size Distribution around the Beam Window

Figure 6 shows the bubble radius distribution measured in the vicinity of the beam window. It can be seen that the bubble sizes were concentrated outstandingly in the range less than 100 μm in radius and only a few bubbles were seen in the larger range at both flow rates of 5 and 7.5 L/s. This observation is also consistent with the calculation result shown in Fig. 5.

The curve for 7.5 L/s shows that the number of bubbles at position E, which is at the far side from the beam window, was larger than that at position D. The reason is considered to be the extra supply of bubbles from channel #2, which is shown in Fig. 2. In the preliminary bubble flow simulation carried out before,[9)] the mercury flow from channel #2 encounters the mercury flow from channel #1 near the beam window, and the bubbles from channel #2 flow through the area of position E.

In the actual mercury flow, flowing distances and sizes of bubbles will be affected by the flow turbulence and bubble coalescences. These influences will be investigated further in the future. The good findings were that the bubbles observed near the beam window had the ideal size for our purpose to suppress the pressure wave, and the bubble number was enhanced by the extra supply from channel #2. In the actual

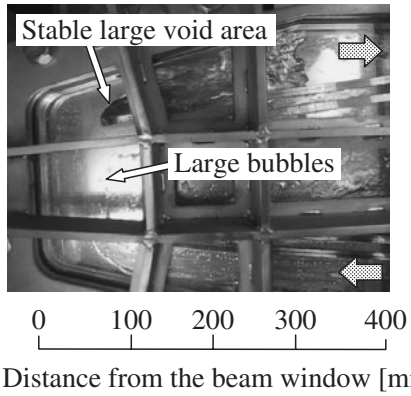

Fig. 7 Top view of bubble flow (Mercury flow rate: 5 L/s)

mercury target, it is expected that more bubbles will be transported rapidly to the beam window due to the higher mercury flow rate of 11.4 L/s. The dotted line in Fig. 5 shows that bubbles with the radius less than 140 μm can reach the beam window.

3. Behavior of Large Bubbles Observed in the Experiment

We observed an unexpected phenomenon in the experiment, which might pose a significant effect on the cooling performance of mercury for the vessel wall. **Figure 7** shows the top view of the bubble flow in the case of a mercury flow rate of 5 L/s. It can be seen that a stable large void area was formed at the downstream side of the flow vane. This void area was formed clearly by the accumulation of bubbles at the flow separation area. As the flow rate was increased, the size of the void area became smaller, and it disappeared at mercury flow rates larger than 6 L/s. Because the heat generation density at the forefront tip of the flow vane is large due to the direct irradiation of the proton beam, the generation of void area is considered to cause the thermal stress of the flow vane with the degradation of the cooling performance. Based on the experience from this experiment, it can be considered that such a void area is not likely to appear under the flow rate of 11.4 L/s of the actual target. However, the fundamental condition for this void generation must be investigated quantitatively in order to confirm that the void area will not be generated in the actual target. The force balance between the mercury surface tension and the inertia of mercury flow might be one of the elements to explain this phenomenon.

Large bubbles with radii from several to ten mm, which were formed by the coalescence of injected small bubbles, were strongly affected by the centrifugal force of the flow channel curvature near the beam window, and the stream line passed through the innermost area of the curvature. It can be seen in Fig. 7 that large bubbles were flowing through the area around 87 mm apart from the beam window. Because the heat generation density in the top wall becomes highest in this area, which is 24 W/cm^3, the effect of the intermittent bubble flow on the cooling performance of mercury was evaluated. The estimated temperature rise in the top wall due to the bubble flow was 30°C, which was not so significant.

IV. Summary

Mercury loop tests to inject helium bubbles into a mockup model of the target vessel of J-PARC were carried out to obtain the data of the bubble size distribution in the mercury flow and also to investigate the bubble flow phenomena in the actual target size. Only the bubbles in the range smaller than 300 μm in radius, which are of our concern, were investigated. As a result, bubbles in the range of radius from 10 to 150 μm, which are the ideal size for our purpose to suppress the pressure wave, were transported to the peak heat load area near the beam window, where the bubbles should be distributed. It was found that the bubbles larger than 150 μm in radius were removed from the distribution by buoyancy at the early stage after the bubble injection, and only the smaller bubbles could be transported downstream. Attention to the effect of bubbles on the cooling performance of the target vessel was raised by the experiment. These results will be reflected in the design of the target vessel that can suppress the pressure wave.

Acknowledgements

The authors would like to acknowledge the support of Mr. Miyamoto and Mr. Miyo who helped us in processing the images.

References

1) S. Nagamiya, "J-PARC project in Japan," *Nucl. Phys. A*, **774**, 895–898 (2006).
2) M. Futakawa, T. Naoe, C. C. Tsai, H. Kogawa, S. Ishikura, Y. Ikeda, H. Soyama, H. Date, "Pitting damage by pressure waves in a mercury target," *Nucl. Mater.*, **343**, 70–80 (2005).
3) M. Futakawa, T. Wakui, H. Kogawa, Y. Ikeda, "Pressure wave issues in high power mercury target," *Nucl. Instrum. Methods A*, **562**, 676–679 (2006).
4) K. Okita, S. Takagi, Y. Matsumoto, "Propagation of pressure waves, caused by a thermal shock, in liquid metals containing gas bubbles," *J. Fluid Sci. Technol.*, **3**, 116–128 (2008).
5) M. Futakawa, H. Kogawa, S. Hasegawa, M. Ida, K. Haga, T. Wakui, T. Naoe, N. Tanaka, Y. Matsumoto, Y. Ikeda, "R&D on pressure-wave mitigation technology for pulsed high-power mercury targets," *Proc. ICANS-XVIII* (2007).
6) M. Ida, T. Naoe, M. Futakawa, "Suppression of cavitation inception by gas bubble injection: A numerical study focusing on bubble-bubble interaction," *Phys. Rev. E*, **76**, 046309 (2007).
7) T. Naoe, M. Ida, M. Futakawa, "Cavitation damage reduction by microbubble injection," *Nucl. Instrum. Methods A*, **586**, 382–386 (2008).
8) F. N. Peebles, H. J. Garber, "Studies on the motion of gas bubbles in liquids," *Chem. Eng. Prog.*, **49**, 88–97 (1953).
9) K. Haga, H. Kogawa, T. Wakui, T. Naoe, M. Futakawa, S. Yamazaki, N. Tanaka, "Bubble flow simulations in target vessel," *Nucl. Instrum. Methods A*, **600**, 64–67 (2009).